


## Article

# Microstructures, Mechanical Properties and Transformation Behavior in Ni<sub>49.6</sub>Ti<sub>35.4</sub>Hf<sub>15</sub> Alloy Produced with High-Pressure Torsion

Jintao Zhang <sup>1</sup>, Shibo Wang <sup>1</sup>, Hua Ding <sup>1,2,\*</sup>, Peng Hu <sup>1</sup>, Yi Huang <sup>3,4,\*</sup>  and Yu Zhang <sup>2</sup>

<sup>1</sup> School of Materials Science and Engineering, Northeastern University, Shenyang 110819, China; 1290712714@126.com (J.Z.); 13224203500@163.com (S.W.); 17855964431@163.com (P.H.)

<sup>2</sup> Key Laboratory of Light Structural Materials of Liaoning Province, Northeastern University, Shenyang 110819, China; humanbeing1989@126.com

<sup>3</sup> Department of Design and Engineering, Faculty of Science and Technology, Bournemouth University, Poole, Dorset BH12 5BB, UK

<sup>4</sup> Materials Research Group, Department of Mechanical Engineering, University of Southampton, Southampton SO17 1BJ, UK

\* Correspondence: dingh@smm.neu.edu.cn (H.D.); yhuang2@bournemouth.ac.uk (Y.H.)

**Abstract:** High-pressure torsion (HPT) was applied for the Ni<sub>49.6</sub>Ti<sub>35.4</sub>Hf<sub>15</sub> (at.%) alloy up to 1/4, 2 and 16 turns under a pressure of 4.0 GPa. The samples were examined using X-ray diffraction (XRD), transmission electron microscope (TEM) and microhardness measurements. The results indicate that the mixture of an amorphous and nanocrystalline microstructure developed in the investigated NiTiHf alloy as the number of HPT turns was increased to two. The average hardness of the samples increased from 330 Hv to 500 Hv after 16 turns of HPT. Very fine martensite developed when the HPT-processed samples were annealed at 550 °C and the finer microstructures were attained with higher HPT turns. Differential scanning calorimetry (DSC) tests were performed in the post-HPT annealing samples to clarify the transformation behavior after severe plastic deformation in HPT and subsequent annealing, so as to provide an experimental basis for the application of the shape memory alloy. The transformation temperature of the alloy decreased remarkably when the number of turns of HPT reached 16. It is suggested that the deformation extent and annealing temperatures should be considered in order to maintain a high transformation temperature while utilizing the strengthening effect of HPT in the NiTiHf alloy.

**Keywords:** NiTiHf alloy; high-pressure torsion; microstructure; mechanical property; transformation behavior



**Citation:** Zhang, J.; Wang, S.; Ding, H.; Hu, P.; Huang, Y.; Zhang, Y. Microstructures, Mechanical Properties and Transformation Behavior in Ni<sub>49.6</sub>Ti<sub>35.4</sub>Hf<sub>15</sub> Alloy Produced with High-Pressure Torsion. *Crystals* **2023**, *13*, 1246. <https://doi.org/10.3390/cryst13081246>

Academic Editor: Vladimir I. Zverev

Received: 5 July 2023

Revised: 19 July 2023

Accepted: 7 August 2023

Published: 12 August 2023



**Copyright:** © 2023 by the authors. Licensee MDPI, Basel, Switzerland. This article is an open access article distributed under the terms and conditions of the Creative Commons Attribution (CC BY) license (<https://creativecommons.org/licenses/by/4.0/>).

## 1. Introduction

In recent years, research into shape memory alloys has aroused much attention due to their application as potential materials in the field of sensors and actuators. NiTi alloys exhibit unique superelasticity and shape memory effects, being the most well-known shape memory alloys (SMAs), and they are the most widely used and commercially available SMAs. The main disadvantage of these alloys is that they demonstrate low dislocation shear stresses due to their volume effects during martensite transformation [1]. Severe plastic deformation (SPD) is an efficient way to refine the microstructure of metallic materials and grain refinement can effectively enhance the strengths of materials [2]. Among different SPD methods, high-pressure torsion (HPT) can afford the highest strain on the processed materials and has been successfully utilized in NiTi SMA processing. The microstructures, mechanical properties and transformation behavior of the materials can be tailored by combining post-HPT annealing treatment with HPT [3–9].

NiTi alloys exhibit a very desirable shape memory effect; however, their transformation temperatures are often lower than 100 °C, which limits their applications. In order to raise

the transformation temperatures of the NiTi alloys, ternary elements have been suggested such as Pd, Au, Pt, Hf and Zr [10–16]. In comparison to alloying with Au and Pt, NiTiHf high-temperature shape memory alloys have attracted much attention as they possess higher transformation temperatures and exhibit considerable shape memory effects and superelasticity at lower costs [15,16]. However, one of the disadvantages in TiNiHf alloys is their low dislocation shear stress [17,18]. Recently, some HPT works have been carried out in TiNiHf alloys for the purpose of enhancing their strength. Shuitcev et al. processed  $\text{Ti}_{29.7}\text{Ni}_{50.3}\text{Hf}_{20}$  shape memory alloys via HPT with turns of 1/2, 1 and 3 and investigated the microstructures of the samples with post-HPT annealing [17]. They reported the formation of nanocrystalline and ultrafine grains after HPT and annealing and applied the Hall–Petch relationship to describe the relationship between the strength and grain size of the material. Ren et al. investigated the role of temperature in the microstructural evolution of HPT-processed NiTiHf shape memory alloys and discussed the difference in the microstructures developed with different HPT processing temperatures [18].

Although there have been several studies into the ternary NiTiHf SMAs processed via HPT, there is little research into the relationship between transformation behavior and microstructure after HPT plus PDA (post-deformation annealing). In particular, there have been no reports on the effects of large HPT turns on the transformation behaviors of ternary NiTiHf SMAs. Therefore, it is very important to clarify the effects of the extent of deformation on microstructural evolution and transformation behavior for practical applications of NiTiHf SMAs. In the present work, NiTiHf SMA samples were processed via different numbers of HPT turns plus PDA. The microstructures were characterized via XRD and TEM. In addition, DSC examinations were carried out to study the transformation behavior of the alloy. By exploring the effect of HPT plus the PDA process on the microstructural evolution and transformation behavior of the materials, it will be possible to provide new insights into the design of SPD schedules and subsequent annealing treatment for the fabrication of NiTiHf ternary SMA materials with high performance.

## 2. Experimental

Previous research has indicated that the transformation temperature can be elevated only when the Hf concentration in NiTiHf alloys is higher than 10% [19]. Hence, a NiTiHf alloy with a nominal composition of 49.6Ni-35.4Ti-15Hf (at.%) was chosen in the present work. The material was prepared using a vacuum induction furnace. The ingot was homogenized at 850 °C for 12 h. The disk samples for HPT processing were cut into 10 mm in diameter and 0.7~0.8 mm in thickness using a wire cutting machine. The samples were processed via HPT up to 1/4, 2 and 16 turns at room temperature under a pressure of 4.0 GPa. The principle of the HPT processing [20] is illustrated schematically in Figure 1. To perform HPT testing, a sample was placed in the depression on the upper surface of the lower anvil, the anvils were brought together to impose a pressure,  $P$ , and torsional straining was then achieved by rotating the lower anvil at a rotational speed of 1 rpm [20].

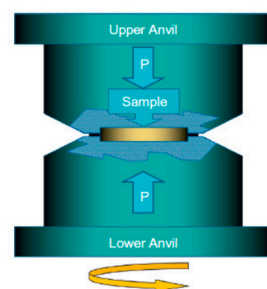


Figure 1. Schematic diagram of processing in HPT [20].

The equivalent strain could then be determined as [21] follows:

$$\gamma = \frac{2N\pi r}{h} \quad (1)$$

$$\varepsilon = \frac{2}{\sqrt{3}} = \ln\left(\frac{\gamma}{2} + \sqrt{1 + \frac{\gamma^2}{4}}\right) \quad (2)$$

where  $r$  is the distance from the disk sample center,  $N$  is the number of revolutions,  $\gamma$  is the shear strain and  $h$  is the final thickness of the sample. The equivalent strains of the experimental samples with different numbers of HPT turns along the radius direction are plotted in Figure 2. The equivalent strain increased as the radius of the sample increased. Moreover, it could be found that the equivalent strain increased with the increasing HPT turns.

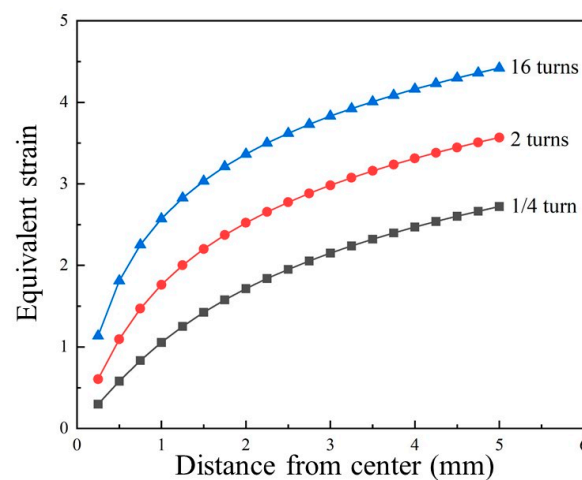


**Figure 2.** Equivalent strain distribution of the experimental samples with different numbers of HPT turns along the radius direction.

The samples after HPT were annealed at 450 °C, 500 °C and 550 °C for 2 h, respectively, and then water quenched.

Differential scanning calorimetry (DSC) experiments were carried out on a TA DSC25 instrument in an atmosphere of helium. The as-homogenized and HPT + PDA samples were heated with a heating rate of 15 °C/min from 25 °C to 350 °C, held for 3 min and then cooled with a cooling rate of 15 °C/min to room temperature.

Vickers microhardness was measured using a FM-700 tester. The load of the indenter was 0.5 kg and the loading time was 10 s.

The samples for XRD examination were extracted from the disk samples using a wire cutting machine and then mechanically ground. The XRD examination was conducted using Smart Lab 9 kW with a target of Cu. The angle of X-ray diffraction was 10°–90° and the XRD scanning speed was 5°/min.

The transmission electron microscope (TEM) samples of 3 mm in diameter were cut off from the HPT samples using a wire cutting machine. The samples were ground to a thickness of 50 µm and then processed via twin-jet electropolishing using Struers TenuPol-5 equipment. The electropolishing solution was HClO<sub>4</sub>:C<sub>2</sub>H<sub>5</sub>OH = 1:9. After twin-jet electropolishing, the samples were carefully polished via an ion beam using Gatan 695 equipment. The samples were firstly polished with the angle of ±5° at the working voltage of 4.5 keV, and then with the angle of ±4.5° at the working voltage of 4.2 keV. The microstructures of the HPT-processed samples were examined via TEM using FEI G 20 equipment.

### 3. Results and Discussion

#### 3.1. Microhardness

Figure 3 shows the microhardness evolution in the as-homogenized and HPT-processed samples. The microhardness (Hv) distributions along the radius of the HPT-processed disk samples showed that the maximum value of Hv was attained at the edge and the minimum value was attained in the center part of the samples. The microhardness of the samples increased from 350 Hv of the as-homogenized state (denoted as Turn 0 in Figure 3) to the average value of 447 Hv after 1/4 turns, and then to 478 Hv after 2 turns with a moderate enhancement. With the further increase in HPT turns to 16, the average hardness increased to over 500 Hv.

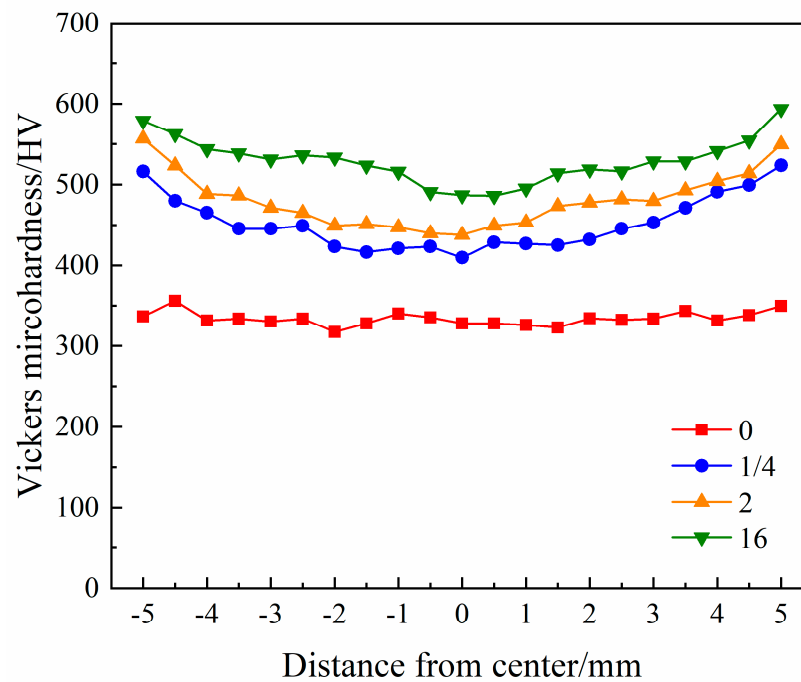


Figure 3. Microhardness distributions along the radius of disks.

Table 1 shows the microhardness values of the samples with different numbers of HPT turns at disk center, half-radius and edge. It is noticed that the microhardness difference between the half-radius and the edge obviously decreases in the 16-turns sample.

Table 1. Microhardness values at disk center, half-radius and edge.

| N   | Microhardness (Hv) |               |               |
|-----|--------------------|---------------|---------------|
|     | Area               |               |               |
|     | Center             | Half-Radius   | Edge          |
| 0   | 330.17 ± 4.97      | 332.95 ± 0.86 | 337.12 ± 0.77 |
| 1/4 | 420.48 ± 11.06     | 447.36 ± 1.92 | 489.73 ± 9.69 |
| 2   | 442.37 ± 7.00      | 473.67 ± 8.35 | 518.69 ± 4.90 |
| 16  | 488.03 ± 2.90      | 526.17 ± 9.90 | 558.28 ± 3.97 |

#### 3.2. Microstructures

Figure 4 shows the XRD patterns of the as-homogenized sample and samples after HPT processing. The as-homogenized microstructure was mainly martensite, including (002)<sub>M</sub>, (11-1)<sub>M</sub> and so on. After HPT processing, a broadening in part of the diffraction reflections of the material can be observed. During the HPT process, the densities of dislocations and grain boundaries increased and the grains were refined. The lattice structures were

highly distorted and the samples after HPT were in a non-equilibrium state. The increase in the dislocations and the grain refinement could make contributions to the broadening of the diffraction peaks [4]. As the number of HPT turns increased, the broadening of the diffraction became more obvious. It could also be found that amorphization occurred in the two-turns sample. The fraction of the amorphous phase increased further in the 16-turns sample, showing an obviously higher (100)<sub>B2</sub> peak.

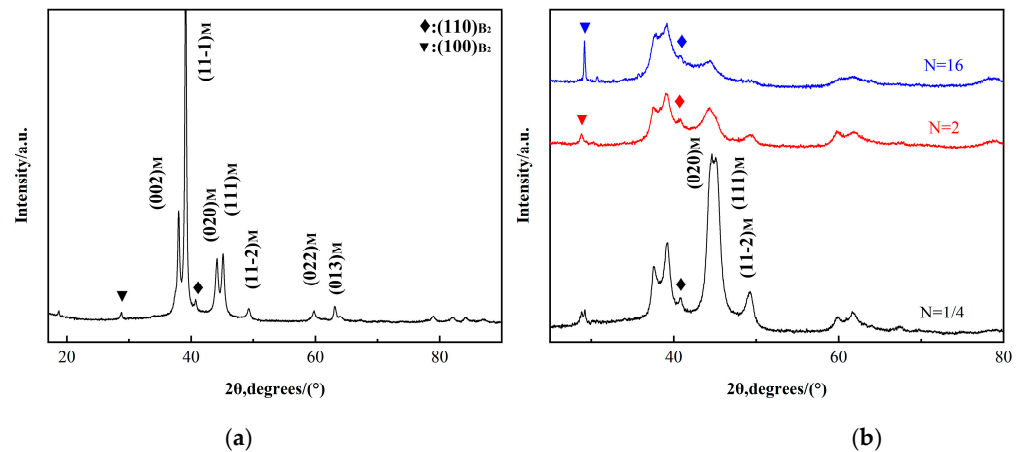


**Figure 4.** XRD patterns before and after HPT. (a) As-homogenized; (b) after HPT.

The microstructures after HPT processing were characterized using TEM, as shown in Figure 5. Before HPT processing, the as-homogenized material showed a fully martensitic microstructure (Figure 5a). The microstructure after 1/4 turns of HPT treatment is given in Figure 5b. The SAED pattern confirmed that the martensitic microstructure was retained. Moreover, the sample demonstrated a deformed microstructure with a high density of dislocations. As the number of HPT turns increased to 2 and 16, a majority of amorphous microstructures developed in the investigated samples due to the accumulation of a high equivalent strain, as confirmed via the halo diffuse ring in the SAED pattern. In addition, a small amount of nanocrystalline microstructures were also found, which could be verified via the crystalline diffraction patterns in the SAED pattern.

During severe plastic deformation such as ECAP and HPT, bulk amorphous NiTi was produced, and it was assumed that the periodicity of the atom arrangement could be destroyed and the formation of the amorphous phase was caused by the increase in defects, such as dislocations and grain boundaries; at the same time, the relaxation processes were difficult [22]. Both dislocations and grain boundaries can store energies, which drive the formation of the crystalline-to-amorphous transformation in NiTi-based alloys.

Several investigations have shown that HPT deformation led to the amorphization in binary TiNi alloys [3–6,8,9]. In some cases, the amorphization was complete [3,8], while nanocrystals were embedded in an amorphous matrix in other cases [4–6,9]. In NiTiHf SMA, there is a report that the amorphous phase formed in an HPT-processed Ti<sub>29.7</sub>Ni<sub>50.3</sub>Hf<sub>20</sub> alloy after three turns of HPT processing [17] and a mixture of the amorphous phase and nanocrystalline microstructure was attained. It was revealed that the tendency of the ternary NiTiHf alloy to form an amorphous microstructure under HPT was higher than that of a binary TiNi alloy due to the more defective structure of martensite in the as-homogenized material [17]. It was estimated that both the energy stored in dislocations and at grain boundaries contribute significantly to driving the crystalline-to-amorphous transformation in NiTi alloys [23], which also implies that martensite is more suitable for amorphization than that of austenite due to its higher defect density. In the present case, the microstructure before HPT was mainly martensite and amorphous phase formed when the HPT turns increased to two, which is similar to the results reported in Ref. [17].

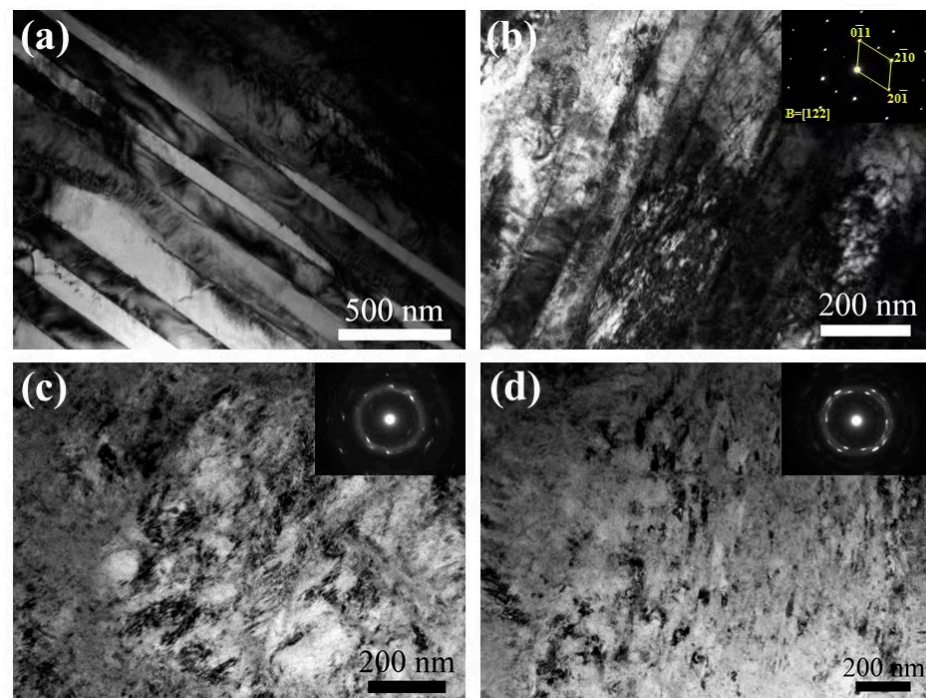


**Figure 5.** Microstructures of the  $\text{Ni}_{49.6}\text{Ti}_{35.4}\text{Hf}_{15}$  alloy prior to and after HPT: (a) as-homogenized; (b) HPT ( $N = 1/4$ ); (c) HPT ( $N = 2$ ); (d) HPT ( $N = 16$ ).

As the formation of the amorphous phase is important for the formation of nanocrystalline grains in the subsequent annealing processes, it is significant to reveal the dynamic feature of the amorphization process. There are some reports to reflect the amorphization process in TiNi alloys in the view of dynamics [24]. The fractions of amorphous phase via DSC and TEM for a TiNi binary alloy in cold rolling were investigated and it was revealed that the volume fraction of the amorphous phase increased linearly with strains [24]. The strain here was not very high ( $\sim 2.0$ ). XRD results were also used to study the extent of the amorphous phase and  $\{110\}_{\text{B2}}$  X-ray line half-width vs. the number of revolutions  $N$  to reveal the dynamic feature of amorphization in the HPT process of the TiNi binary alloy [5]. However, there have been no reports on amorphization in the HPT-processed TiNiHf ternary alloy. In order to reveal the amorphous transformation of the experimental material during HPT processes, the volume fractions of crystalline were examined via XRD. The volume fraction of crystalline vs. the applied HPT turns is given in Figure 6. The results showed that the volume fraction of crystalline decreased as the applied HPT turns increased. To be explicit, the sample without HPT processing exhibited an amount of  $\sim 97\%$  in the volume fraction of crystalline, showing an almost fully crystallized microstructure after initial annealing at  $850\text{ }^\circ\text{C}$  for 12 h on the as-received ingot. There existed a remarkable decrease in the volume fraction of crystalline after  $1/4$  turns. This was because the equivalent strain of  $1/4$  turns was 1.952, which facilitated the occurrence of the amorphous transformation. The corresponding TEM result (Figure 5b) showed a deformed microstructure with a high density of dislocations in the sample with  $1/4$  HPT turns, revealing that severe plastic deformation occurred, and consequently led to the formation of an amorphous microstructure. When the number of HPT turns was increased to two, a remarkable further decrease could be seen in the volume fraction of crystalline. Given that the equivalent strain of two turns increased to 4.313, the accumulation of the applied strain was high enough to distort the lattice structure. Therefore, the dramatic amorphous transformation occurred in the sample after two turns, which is in accordance with the TEM result (Figure 5c) showing that an obvious halo diffuse ring could be observed in the SAED pattern. It is noteworthy that when the number of HPT turns was increased to 16, the sample exhibited a slight decrease in the volume fraction of crystalline. Since a large

amount of amorphous transformation was achieved in the sample with less HPT turns, the sample processed with 16 turns demonstrated an exhaustion in the further amorphous transformation, although the equivalent strain of 16 turns was 6.714.

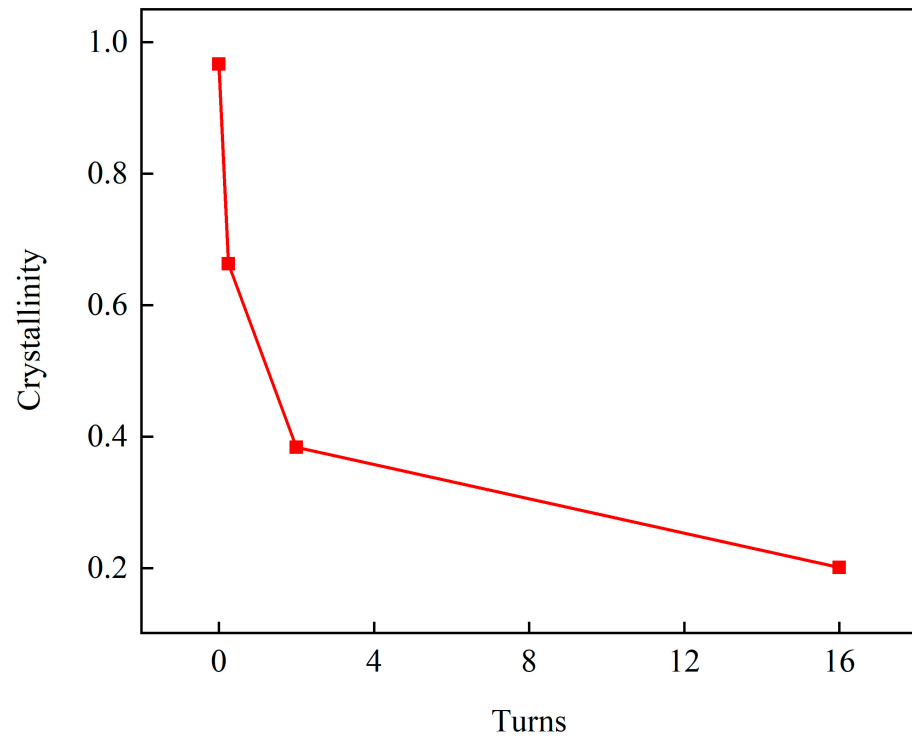


**Figure 6.** The volume fraction of crystalline with different numbers of HPT turns.

Amorphous phase is a meta-stabilized state and its Gibbs energy is high. In suitable conditions, crystallization would occur. Generally, amorphization plus annealing is a method for gaining an ultrafine microstructure in severe plastic deformation processes and subsequent heat treatment. TEM micrographs of the investigated samples after annealing at 550 °C with different numbers of HPT turns are given in Figure 7. The results show that a nano-scaled martensite microstructure was obtained in all of the investigated samples. In comparison to the sample with 1/4 turns, the samples with 2 and 16 turns exhibited a more-refined microstructure, which can be ascribed to their more significant recrystallization during the annealing processes as a result of the higher equivalent strains induced via HPT.

### 3.3. Transformation Behavior

The DSC curves of the as-homogenized TiNiHf alloy annealed at different temperatures are shown in Figure 8. The transition temperature were noticed in Figure 8. Tangential points are phase transition temperature. It is indicated that the annealing temperatures exert no obvious influence on the transformation behavior of the as-homogenized samples. The  $M_s$ ,  $M_f$ ,  $A_s$  and  $A_f$  of the TiNiHf alloys are 198, 164, 230 and 260 °C, respectively. In the 49.5% NiTi binary alloy [25],  $M_s$ ,  $M_f$ ,  $A_s$  and  $A_f$  were 78, 55, 83 and 107 °C, respectively. Therefore, it is demonstrated that the transformation temperatures in the TiNiHf alloy were much higher than the ones in the NiTi binary alloy.

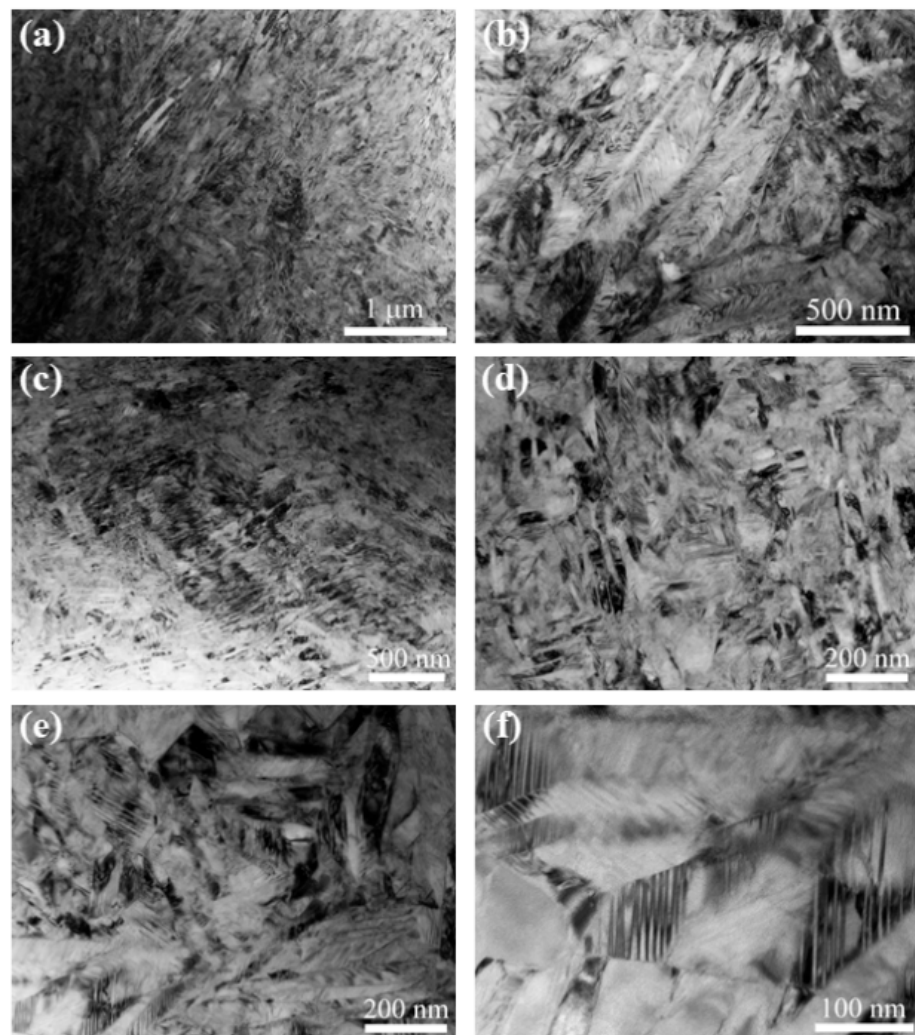


**Figure 7.** Microstructures of the  $\text{Ni}_{49.6}\text{Ti}_{35.4}\text{Hf}_{15}$  alloy after HPT and post-HPT annealing ( $550\text{ }^{\circ}\text{C}$ ): (a,b) HPT ( $N = 1/4$ ); (c,d) HPT ( $N = 2$ ); (e,f) HPT ( $N = 16$ ).

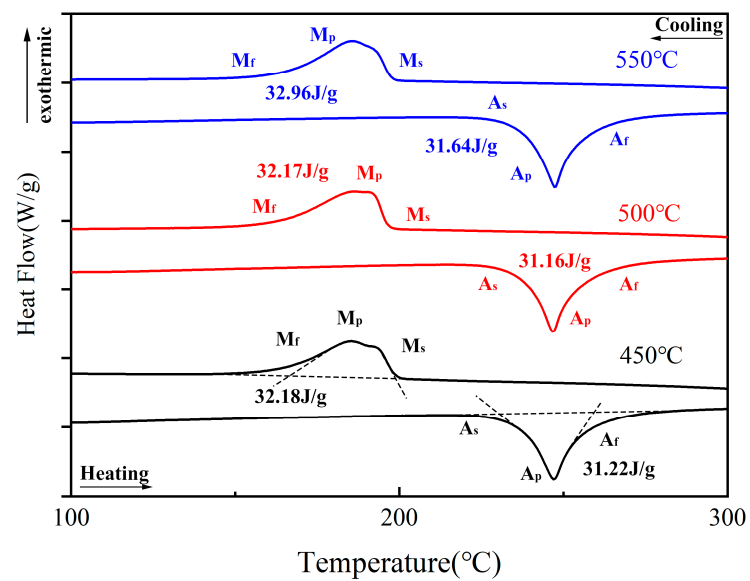


**Figure 8.** DSC results obtained for the as-homogenized TiNiHf alloy.



Figure 9 shows the DSC results obtained for the TiNiHf alloy after HPT ( $N = 1/4, 2, 16$ ) + PDA (post-HPT annealing) and Table 2 lists the corresponding temperatures and enthalpies of the transformation. The transition temperature were noticed in Figure 9. From Table 2, there is a decrease in transformation temperature with the turns of HPT increasing, which indicates the suppression of martensite transformation. It can be found that the values of transition enthalpy decreased as the HPT turns increased, which was connected with the decrease in transformation temperatures in the investigated alloy as well.

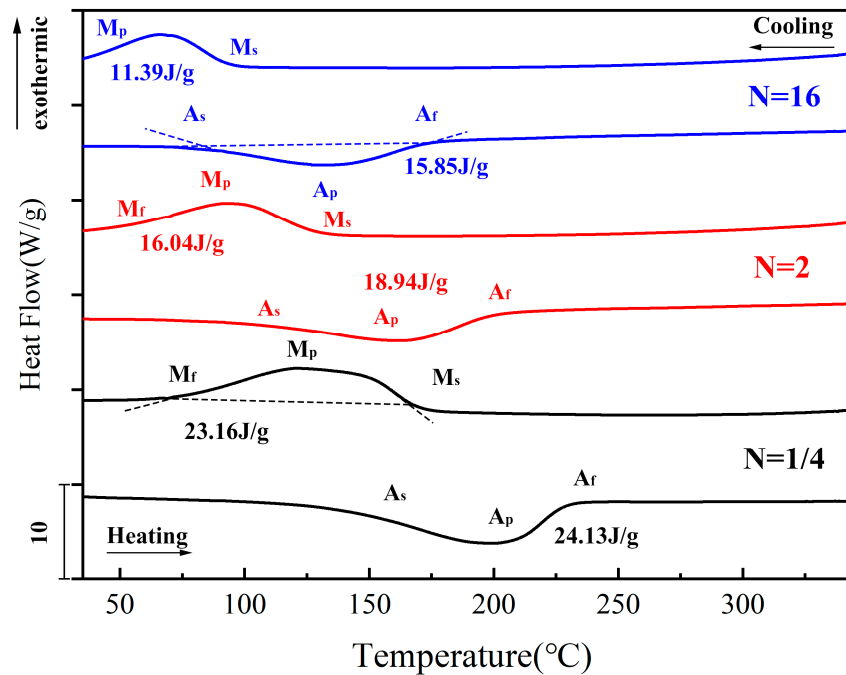


**Figure 9.** DSC results obtained for TiNiHf alloy after HPT ( $N = 1/4, 2, 16$ ) + PDA (annealing at 550 °C).

**Table 2.** Transformation behavior of NiTiHf samples after HPT ( $N = 1/4, 2, 16$ ) plus PDA (annealing at 550 °C).

| N   | Temperature (°C) |       |        |        |        |        | Transition Hysteresis (°C) | Transition Enthalpy, H (J/g) |                       |
|-----|------------------|-------|--------|--------|--------|--------|----------------------------|------------------------------|-----------------------|
|     | $M_s$            | $M_f$ | $A_s$  | $A_f$  | $M_p$  | $A_p$  |                            | $B2 \rightarrow B19'$        | $B19' \rightarrow B2$ |
| 1/4 | 170.76           | 74.91 | 133.10 | 229.53 | 122.37 | 199.34 | 58.77                      | 23.26                        | −24.13                |
| 2   | 130.69           | 62.13 | 96.67  | 201.91 | 93.02  | 162.52 | 71.22                      | 16.04                        | −18.94                |
| 16  | 95.49            | 30.73 | 81.90  | 175.19 | 66.57  | 134.24 | 79.70                      | 11.39                        | −15.85                |

There have been a lot of investigations into the effect of microstructure on the phase transformation behavior of NiTi binary alloys. Waitz [4] processed Ni-50.3 at% Ti using HPT at room temperature and investigated the size effects on martensitic phase transformations in nanocrystalline NiTi shape memory alloys. For comparison, they also studied the coarse-grained NiTi alloy with the same compositions. It was found that the transformation to martensite was suppressed in the nanocrystalline microstructure of NiTi alloys after HPT and heat treatment. In the coarse-grained NiTi alloy,  $M_s$  was 57 °C and  $A_s$  was 65 °C, whereas the  $M_s$  decreased to 46 °C and the  $A_s$  decreased to 17 °C in the nanocrystalline NiTi alloy. It was concluded that in a nanocrystalline NiTi alloy, the martensitic transformation could be suppressed in different ways: via the introduction of elastic strains, via lattice defects or via crystal refinement [26]. It was suggested that the high density of grain boundaries obstructed the growth of martensite and the increase in interface energy was also a cause for the suppression of martensite formation in the nanograins [27].

For the NiTiHf alloy, there are reports on microstructural evolution only related to a small number of turns of HPT processing (one turn in [18] and three turns in [17]), and the transformation behavior after HPT plus PDA (post-deformation annealing) has not been properly investigated. In the present work, it is clearly indicated that the martensite transformation temperature of the TiNiHf alloy decreased with the increase in the number of HPT turns. There is a substantial decrease in the martensite transformation start temperature ( $M_s$ ) from about 200 °C in the as-homogenized sample to about 95 °C in the sample, with 16 turns of HPT in the NiTiHf alloy (shown in Figure 8 and Table 2), which is just a little higher than the one reported in the 49.5% NiTi binary alloy with an  $M_s$  of 78 °C [25]. Based on the results of the TEM analysis in Figure 5, very fine microstructures were achieved after HPT processing, especially in large turns. The decrease in the transformation temperature must be related to the fine microstructure.

It is revealed in Table 2 that the transition hysteresis width increased with the increase in revolutions of HPT. It is suggested that there are two key energy dissipative processes that govern the hysteresis in martensite transformation [28]. One is energy dissipated in the form of friction work, and the other is the dissipation of elastic energy. The magnitude of the total energy dissipation could be reflected in the thermal or stress hysteresis.

It is suggested that the factors influencing the transition hysteresis width include alloying elements, microstructure and extent of pre-deformation [29]. The transition hysteresis width is very sensitive to the compositions in NiTi alloys. It was reported in [30] that the transition hysteresis width was about 17 °C with the Ni concentration being 50.1 at%. When the Ni concentration increased to 51.5 at%, the transition hysteresis width increased to 43 °C, which was caused by the increase in the phase transformation temperature due to the increase in Ni concentrations and the decrease in resistance to the martensite transformation. Different grain sizes were obtained in Ni<sub>49.7%</sub>Ti<sub>50.3%</sub> via hot rolling and equal-channel angular extrusion [31]. The transition hysteresis width was about 36 °C when the grain size was large (40 μm), whereas it was 45–52 °C when the grain size decreased to 0.1–0.3 μm. Therefore, the decrease in grain size resulted in an enlargement of transition hysteresis. Generally, the transition hysteresis width of TiNiHf alloys is relatively large (>50 °C) [28]. It can be deduced that the increase in transition hysteresis width in the samples with a large HPT strain in the present work is due to the refined microstructure.

From the above results, it is clearly indicated that the martensite transformation temperature of the TiNiHf alloy decreased substantially when the number of turns of HPT was high. Our results also show that the decrease in the transformation temperature is much smaller when the annealing temperatures after HPT in the TiNiHf alloy are lower. It is suggested that the combination of HPT and annealing schedules should be optimized to tailor the mechanical properties while maintaining the characteristics of a high-temperature shape memory NiTiHf alloy.

#### 4. Conclusions

In summary, the effects of high-pressure torsion and subsequent annealing on the microstructures, microhardness and phase transformation behavior of a ternary TiNiHf shape memory alloy were investigated. The results from XRD, TEM, DSC and microhardness analysis led to the following conclusions:

- (1) The hardness evolution of the HPT-processed samples shows that the hardness values increase with the number of HPT turns. The average microhardness in the HPT-processed 16-turns sample was over 500 Hv, which is much higher than that in the as-homogenized sample (~330 Hv).
- (2) The XRD and TEM results reveal that HPT processing at room temperature leads to the formation of an amorphous–nanocrystalline mixture in the investigated TiNiHf alloy. Significantly refined martensite was attained when the HPT-processed samples were annealed at 550 °C. Finer microstructures could be obtained with increasing HPT turns.

- (3) For the TiNiHf alloy after HPT plus PDA, the martensite transformation temperature decreased, the transition hysteresis width increased and the transition enthalpy decreased with the increase in HPT revolutions. When the HPT turns increased to 16, the martensite transformation temperature decreased remarkably (with  $M_s$  being less than 100 °C). HPT and annealing schedules need to be optimized to enhance the mechanical properties and simultaneously maintain the good characteristics of high-temperature TiNiHf alloys.

**Author Contributions:** Conceptualization, J.Z., H.D. and Y.H.; methodology, J.Z.; investigation, J.Z., S.W., P.H. and Y.Z.; writing—original draft preparation, J.Z., H.D. and Y.H.; writing—review and editing, J.Z., H.D. and Y.H. All authors have read and agreed to the published version of the manuscript.

**Funding:** This research received no external funding.

**Data Availability Statement:** The data that has been used is confidential. The raw/processed data required to reproduce these findings cannot be shared at this time as the data also forms part of an ongoing study.

**Conflicts of Interest:** The authors declare no conflict of interest.

## References

1. Shuitcev, A.; Vasin, R.N.; Fan, X.M.; Balagurov, A.M.; Bobrikov, I.A.; Li, L.; Golovin, I.S.; Tong, Y.X. Volume Effect upon Martensitic Transformation in Ti<sub>29.7</sub>Ni<sub>50.3</sub>Hf<sub>20</sub> High Temperature Shape Memory Alloy. *Scr. Mater.* **2020**, *178*, 67–70. [\[CrossRef\]](#)
2. Valiev, R.Z.; Islamgaliev, R.K.; Alexandrov, I.V. Bulk Nanostructured Materials from Severe Plastic Deformation. *Prog. Mater. Sci.* **2000**, *45*, 103–189. [\[CrossRef\]](#)
3. Sergueeva, A.V.; Song, C.; Valiev, R.Z.; Mukherjee, A.K. Structure and Properties of Amorphous and Nanocrystalline NiTi Prepared by Severe Plastic Deformation and Annealing. *Mater. Sci. Eng. A* **2003**, *339*, 159–165. [\[CrossRef\]](#)
4. Waitz, T.; Kazykhanov, V.; Karnthaler, H.P. Martensitic phase transformations in nanocrystalline NiTi studied by TEM. *Acta Mater.* **2004**, *52*, 137–147. [\[CrossRef\]](#)
5. Prokoshkin, S.D.; Khmelevskaya, I.Y.; Dobatkin, S.V.; Trubitsyna, I.B.; Tatyannin, E.V.; Stolyarov, V.V.; Prokofiev, E.A. Alloy composition, deformation temperature, pressure and post-deformation annealing effects in severely deformed Ti–Ni based shape memory alloys. *Acta Mater.* **2005**, *53*, 2703–2714. [\[CrossRef\]](#)
6. Khmelevskaya, I.Y.; Prokoshkin, S.D.; Dobatkin, S.V.; Tatyannin, E.V.; Trubitsyna, I.B. Studies of composition, deformation temperature and pressure effects on structure formation in severely deformed TiNi-based alloys. *Mater. Sci. Eng. A* **2006**, *438–440*, 472–475. [\[CrossRef\]](#)
7. Singh, R.; Divinski, S.V.; Rösner, H.; Prokofiev, E.A.; Valiev, R.Z.; Wilde, G. Microstructure evolution in nanocrystalline NiTi alloy produced by HPT. *J. Alloys Compd.* **2011**, *509*, S290–S293. [\[CrossRef\]](#)
8. Valiev, R.Z.; Gunderov, D.V.; Lukyanov, A.V.; Pushin, V.G. Mechanical behavior of nanocrystalline TiNi alloy produced by severe plastic deformation. *J. Mater. Sci.* **2012**, *47*, 7848–7853. [\[CrossRef\]](#)
9. Shahmir, H.; Nili-Ahmadabadi, M.; Huang, Y.; Myun Jung, J.; Seop Kim, H.; Langdon, T.G. Shape memory effect in nanocrystalline NiTi alloy processed by high-pressure torsion. *Mater. Sci. Eng. A* **2015**, *626*, 203–206. [\[CrossRef\]](#)
10. Ramaiah, K.V.; Saikrishna, C.N.; Gouthama; Bhaumik, S.K. Microstructure and transformation behavior of Ni<sub>24.7</sub>Ti<sub>50.3</sub>Pd<sub>25</sub> high temperature shape-memory alloy with Sc micro-addition. *Mater. Charact.* **2015**, *106*, 36–43. [\[CrossRef\]](#)
11. Casalena, L.; Bigelow, G.S.; Gao, Y.P.; Benafan, O.; Noebe, R.D.; Wang, Y.; Mills, M.J. Mechanical behavior and microstructural analysis of NiTi-10Au shape memory alloys exhibiting work output above 400 °C. *Intermetallics* **2017**, *86*, 33–44. [\[CrossRef\]](#)
12. Lin, B.; Gall, K.; Maier, H.J.; Waldron, R. Structure and thermomechanical behavior of NiTiPt shape memory alloy wires. *Acta Biomater.* **2009**, *5*, 257–267. [\[CrossRef\]](#) [\[PubMed\]](#)
13. Hsieh, S.F.; Wu, S.K. A Study on Ternary Ti-rich TiNiZr shape memory alloys. *Mater. Charact.* **1998**, *41*, 151–162. [\[CrossRef\]](#)
14. Evirgen, A.; Karaman, I.; Santamarta, R.; Pons, J.; Hayrettin, C.; Noebe, R.D. Relationship between crystallographic compatibility and thermal hysteresis in Ni-Rich NiTiHf and NiTiZr high temperature shape memory alloys. *Acta Mater.* **2016**, *121*, 374–383. [\[CrossRef\]](#)
15. Hayrettin, C.; Karakoc, O.; Karaman, I.; Mabe, J.H.; Santamarta, R.; Pons, J. Two way shape memory effect in NiTiHf high temperature shape memory alloy tubes. *Acta Mater.* **2019**, *163*, 1–13. [\[CrossRef\]](#)
16. Toker, G.P.; Nematollahi, M.; Saghaian, S.E.; Baghbaderani, K.S.; Benafan, O.; Elahinia, M.; Karaca, H.E. Shape memory behavior of NiTiHf alloys fabricated by selective laser melting. *Scr. Mater.* **2020**, *178*, 361–365. [\[CrossRef\]](#)
17. Shuitcev, A.; Gunderov, D.V.; Sun, B.; Li, L.; Valiev, R.Z.; Tong, Y.X. Nanostructured Ti<sub>29.7</sub>Ni<sub>50.3</sub>Hf<sub>20</sub> High temperature shape memory alloy processed by high-pressure torsion. *J. Mater. Sci. Technol.* **2020**, *52*, 218–225. [\[CrossRef\]](#)
18. Ren, Y.; Shuitcev, A.; Gunderov, D.V.; Li, L.; Valiev, R.Z.; Tong, Y.X. The Role of temperature in the microstructural evolution of HPT-processed NiTiHf high-temperature shape memory alloy. *Mater. Lett.* **2022**, *322*, 132484. [\[CrossRef\]](#)

19. Karaca, H.E.; Acar, E.; Tobe, H.; Saghaian, S.M. NiTiHf-based shape memory alloys. *Mater. Sci. Tech.* **2014**, *30*, 1530–1544. [[CrossRef](#)]
20. Xu, C.; Horita, Z.; Langdon, T.G. The evolution of homogeneity in an aluminum alloy processed using high-pressure torsion. *Acta Materialia* **2008**, *56*, 5168–5176. [[CrossRef](#)]
21. Kilmametov, A.R.; Vaughan, G.; Yavari, A.R.; LeMoulec, A.; Botta, W.J.; Valiev, R.Z. Microstructure evolution in copper under severe plastic deformation detected by in situ X-ray diffraction using monochromatic synchrotron light. *Mater. Sci. Eng. A* **2009**, *503*, 10–13. [[CrossRef](#)]
22. Rogachev, S.O.; Sundev, R.V.; Tabachekova, N.Y. High pressure torsion-induced amorphous phase in a multilayer V-10Ti-5Cr/Zr-2.5Nb/V-10Ti-5Cr hybrid material. *Mater. Lett.* **2019**, *234*, 220–223. [[CrossRef](#)]
23. Huang, J.Y.; Zhu, Y.T.; Liao, X.Z.; Valiev, R.Z. Amorphization of TiNi induced by high-pressure torsion. *Philos. Mag. Lett.* **2004**, *84*, 183–190. [[CrossRef](#)]
24. Ewert, J.C.; Bohm, I.; Peter, R.; Haider, F. The role of the martensite transformation for the mechanical amorphisation of NiTi. *Acta Mater.* **1997**, *45*, 2197–2206. [[CrossRef](#)]
25. Mahesh, K.K.; Braz, Fernandes, F.M.; Gurau, G. Stability of thermal-induced phase transformation in the severely deformed equiatomic Ni-Ti alloys. *J. Mater. Sci.* **2012**, *47*, 6005–6014. [[CrossRef](#)]
26. Nakayama, H.; Tsuchiya, K.; Umamoto, M. Crystal refinement and amorphisation by cold rolling in shape memory alloys. *Scripta Mater.* **2001**, *44*, 1781. [[CrossRef](#)]
27. Waitz, T.; Antretter, T.; Fischer, F.D. Size effects on martensitic phase transformations in nanocrystalline NiTi shape memory alloys. *Mater. Sci. Technol.* **2008**, *24*, 934–940. [[CrossRef](#)]
28. Karaca, H.E.; Saghaian, S.M.; Ded, G.; Tobe, H.; Basaran, B.; Maier, H.J.; Noebe, R.D.; Chumlyakov, Y.I. Effects of nanoprecipitation on the shape memory and material properties of an Ni-rich NiTiHf high temperature shape memory alloy. *Acta Mater.* **2013**, *61*, 7422–7432. [[CrossRef](#)]
29. Frenzel, J.; George, E.; Dlouhy, A.; Somsen, C.; Wagner, M.X.; Eggeler, G. Influence of Ni on martensitic phase transformations in NiTi shape memory alloys. *Acta Mater.* **2010**, *58*, 3444–3458. [[CrossRef](#)]
30. Sehitoglu, H.; Hamilton, R.; Maier, H.J.; Chumlyakov, Y. Hysteresis in NiTi alloys. *J. Phys. IV Fr.* **2004**, *115*, 3–10.
31. Kockar, B.; Karaman, I.; Kim, J. Thermomechanical cyclic response of an ultrafine-grained NiTi shape memory alloy. *Acta Mater.* **2008**, *56*, 3630–3646. [[CrossRef](#)]

**Disclaimer/Publisher’s Note:** The statements, opinions and data contained in all publications are solely those of the individual author(s) and contributor(s) and not of MDPI and/or the editor(s). MDPI and/or the editor(s) disclaim responsibility for any injury to people or property resulting from any ideas, methods, instructions or products referred to in the content.